Advances in Radiation Oncology (2018) **3**, 209–215

advances
in radiation oncology

www.advancesradonc.org

Scientific Article

A rapid, computational approach for assessing interfraction esophageal motion for use in stereotactic body radiation therapy planning

Michael L. Cardenas MD, Thomas R. Mazur PhD, Christina I. Tsien MD, Olga L. Green PhD *

Washington University in St. Louis, St. Louis, Missouri

Received 14 March 2017; received in revised form 30 August 2017; accepted 3 October 2017

Abstract

Purpose: We present a rapid computational method for quantifying interfraction motion of the esophagus in patients undergoing stereotactic body radiation therapy on a magnetic resonance (MR) guided radiation therapy system.

Methods and materials: Patients who underwent stereotactic body radiation therapy had simulation computed tomography (CT) and on-treatment MR scans performed. The esophagus was contoured on each scan. CT contours were transferred to MR volumes via rigid registration. Digital Imaging and Communications in Medicine files containing contour points were exported to MATLAB. In-plane CT and MR contour points were spline interpolated, yielding boundaries with centroid positions, C_{CT} and C_{MR}. MR contour points lying outside of the CT contour were extracted. For each such point, $B_{MR}(j)$, a segment from C_{CT} intersecting $B_{MR}(j)$, was produced; its intersection with the CT contour, $B_{CT}(i)$, was calculated. The length of the segment S_{ij}, between $B_{CT}(i)$ and $B_{MR}(j)$, was found. The orientation θ was calculated from S_{ij} vector components:

$\theta = \arctan[(S_{ij})_y / (S_{ij})_x]$

A set of segments $\{S_{ij}\}$ was produced for each slice and binned by quadrant with $0° < \theta \leq 90°$, $90° < \theta \leq 180°$, $180° < \theta \leq 270°$, and $270° < \theta \leq 360°$ for the left anterior, right anterior, right posterior, and left posterior quadrants, respectively. Slices were binned into upper, middle, and lower esophageal (LE) segments.

Results: Seven patients, each having 3 MR scans, were evaluated, yielding 1629 axial slices and 84,716 measurements. The LE segment exhibited the greatest magnitude of motion. The mean LE measurements in the left anterior, left posterior, right anterior, and right posterior were 5.2 ± 0.07 mm, 6.0 ± 0.09 mm, 4.8 ± 0.08 mm, and 5.1 ± 0.08 mm, respectively. There was considerable interpatient variability.

Conclusions: The LE segment exhibited the greatest magnitude of mobility compared with the middle and upper esophageal segments. A novel computational method enables personalized, nonuniform esophageal margins to be tailored to individual patients.

Conflicts of interest: None.

* Corresponding author. Washington University in St. Louis, 4921 Parkview Place, Lower Level, St. Louis, MO 63139.
E-mail address: ogreen@wustl.edu (O.L. Green).

https://doi.org/10.1016/j.adro.2017.10.003

Introduction

Esophagus movement is difficult to account for in stereotactic body radiation therapy (SBRT) treatment planning and its presence can compromise otherwise normal dose-volume histogram accuracy. Esophagus movement results in large part from the respiratory cycle, cardiac motion, and peristalsis. The extent of esophageal motion has been described previously in the literature.

Symptomatic, radiation-induced esophagitis is a potentially severe complication of radiation therapy. Symptoms can lead to treatment interruption, potentially compromising overall treatment efficacy.[1] Delayed esophageal complications, including severe ulceration, perforation, or fistula formation,[2] are uncommon but are increasingly reported after SBRT. With a trend toward increased use of high-dose-per-fraction SBRT and systemic chemotherapies, esophagus injury significance and the need to mitigate it is of increasing importance.

Several dosimetric parameters have been shown to be predictive of toxicity. In conventional fractionation, esophagus volumes receiving >40 to 50 Gy correlate with acute esophagitis.[3] However, in SBRT, the maximum doses to 1 cc (D_{1cc}), 2.5 cc, 5 cc, and the maximum point dose have been shown to predict acute esophagitis.[4-6] The late toxicity of fistula formation has been shown to be related to D_{1cc} exceeding 50 Gy, with patients receiving adjuvant anti-angiogenic therapies being at particularly high risk.[7]

Several prior studies have used various computed tomography (CT)-based methods for quantifying esophageal motion and have relied for the most part on digital calipers for measurements in the medial-lateral and anterior-posterior directions in a sample of axial planes spanning the length of the organ.[8-11] One study has modeled esophageal motion secondary to the cardiac cycle by tracking voxel-for-voxel trajectories in the left-right, anterior-posterior, and superior-inferior directions.[12]

MR imaging (MRI) offers high contrast imaging of soft tissue. MR-guided radiation therapy enables daily imaging without exposing patients to additional radiation.[13,14] In this study, we retrospectively analyzed esophageal motion during SBRT treatments for patients treated on an MR-guided radiation therapy system. We evaluated esophageal interfraction motion using the initial planning CT scan as well as subsequent daily pretreatment MR scans. In the quantification of this motion, we introduce a novel computational method that analyzes MR scans slice by slice in all radial directions to yield a comprehensive characterization of esophageal motion.

Methods and materials

Patients

This was an institutional review board–approved retrospective study. A total of 7 consecutive patients were treated with thoracic SBRT on an MR-guided radiation therapy system that consisted of an annular gantry including 3 Co-60 sources positioned 120 degrees apart and a 0.35 Tesla whole-body MRI scanner (Viewray, Cleveland, OH).[12] Patient factors including gross tumor volume location, tumor type, dose, and fractionation are summarized in Table 1. Briefly, 3 patients with early-stage non-small cell lung cancer were treated with curative intent, 1 patient was treated for extensive-stage small cell lung cancer, and 3 patients were treated for metastatic disease.

Image acquisition

A planning CT simulation scan and daily on-treatment MR scans were acquired for each patient. CT scans were acquired on a 64-slice CT scanner (Brilliance 64, Philips Medical Systems, Andover, MA) at 120 kVP with a 50 cm field of view, 0.98×0.98 mm^2 in-plane resolution, and 3 mm slice thickness. CT acquisitions were performed during end-exhale breath hold. MR acquisitions were done during free breathing. The on-treatment MR scans were obtained for each patient at fractions corresponding to the beginning, middle, and end of treatment. For convenience, we refer to these scans as fraction 1, fraction 2, and fraction 3, respectively.

For all patients, the esophagus was contoured on transverse slices on both CT and MR volumes spanning from

Table 1 Patient factors summary

Patient No.	Age (y)	Tumor type	Tumor location	Dose (Gy)	Fractions (n)
1	80	NSCLC adenocarcinoma	Right hilum	60	10
2	73	Extensive-stage small cell lung cancer	Left upper lobe	46	15
3	75	NSCLC adenocarcinoma	Left lower lobe	30	5
4	48	Oligometastatic rectal adenocarcinoma	Right hilum	60	12
5	31	Synovial carcinoma (right knee metastasis)	Subcarina/right hilum	60	12
6	71	NSCLC adenocarcinoma	Left upper lobe	62.5	10
7	75	Undifferentiated pleomorphic sarcoma (right hip metastasis)	Mediastinal lymph node	62.5	10

NSCLC, non-small cell lung cancer.

the cricoid to the gastroesophageal junction. Esophagus contours from CT simulation were then transferred to MR volumes via rigid registration using bony anatomy to guide the alignment. MR volumes were acquired using a balanced, steady-state, free precession sequence (TrueFISP, Siemens, Munich, Germany) with repetition and echo times of 3 and 1.27 ms, respectively. MR volume in-plane spatial resolution was 1.5×1.5 mm^2, and slice thickness in-plane spatial resolution was 3 mm. Thus, a line between 2 voxels has an uncertainty of approximately ±1.5 mm. The nominal field of view was $54 \times 47 \times 43$ cm^3 for 4 patients and $40 \times 40 \times 43$ cm^3 for the remaining 3 patients. Digital Imaging and Communications in Medicine structure files containing coordinates for each contour were exported to MATLAB (MathWorks, Natick, MA).

Slice-by-slice setup geometry

An array was constructed and populated with the coordinates from contours in the image coordinate system (Fig 1). Spline interpolation was applied between contour point coordinates to resample contours with a higher point density while preserving conformality to esophageal anatomy.

Sampling density S within a given slice i was determined as a function of the MR contour perimeter P_{MRi} on that slice and the median MR contour perimeter $P_{MR\mu}$ for the fraction by the formula $S = 100 \cdot (P_{MRi} / P_{MR\mu})$.

Both CT and MR contour boundaries were used to create image masks from which the centroid positions C_{CT} and C_{MR}, respectively, could be calculated. To characterize the differences between contours slice by slice, we first extracted all points on an MR contour lying outside the CT contour boundary. These points we defined as $B_{MR}(j)$. For each $B_{MR}(j)$, a segment originating from C_{CT} and intersecting $B_{MR}(j)$ was produced. The segment was extended beyond $B_{MR}(j)$ to enable the detection of any other points on the MR contour boundary that may lie in the same orientation relative to C_{CT}. If the segment intersected more than 1 point on the MR contour, quantitative analysis was performed only on the point lying furthest from C_{CT}. The segment intersection with the CT contour, $B_{CT}(i)$, was then calculated. The length of the segment S_{ij} between $B_{CT}(i)$ and $B_{MR}(j)$, defined as S_{ij}, represented a local margin expansion for a specific direction. Figure 2 illustrates this process.

This procedure yielded a set of segments $\{S_{ij}\}$ within a given slice for all points $B_{CT}(i)$ identified within the slice. The orientation θ of each segment could be simply inferred relative to a fixed axis by

$$\Theta = \arctan\left[\left(S_{ij}\right)_y / \left(S_{ij}\right)_x\right]$$

in which $(S_{ij})_x$ and $(S_{ij})_y$ denote vector components of a particular segment. Binning these orientations slice by slice enables the characterization of anisotropic variation along the length of the esophagus.

Statistical analysis

Measurements were binned by segments into upper, middle, and lower thirds of the esophagus, which were defined by dividing the length of the esophagus from the cricoid to the gastroesophageal junction into equal thirds. We found that these partitions roughly corresponded to levels

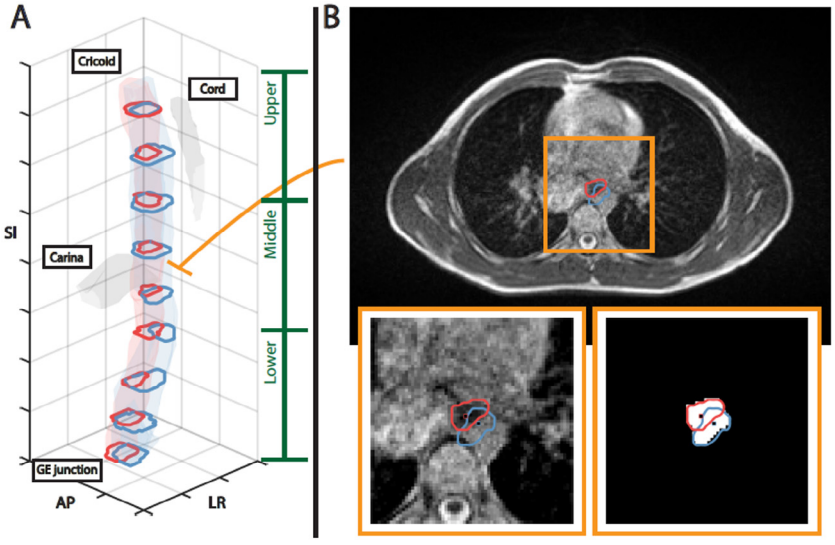

Figure 1 Setup geometry. (a) An array is constructed with a size that is consistent with the magnetic resonance volume. The coordinates from contours in the image coordinate system populate the array (computed tomography based in blue, magnetic resonance based in red). (b) The coordinates are spline interpolated and resampled to improve measurement density. This process yields contour boundaries that are used to create image masks. Image masks enable the calculation of the centroid position for each contour.

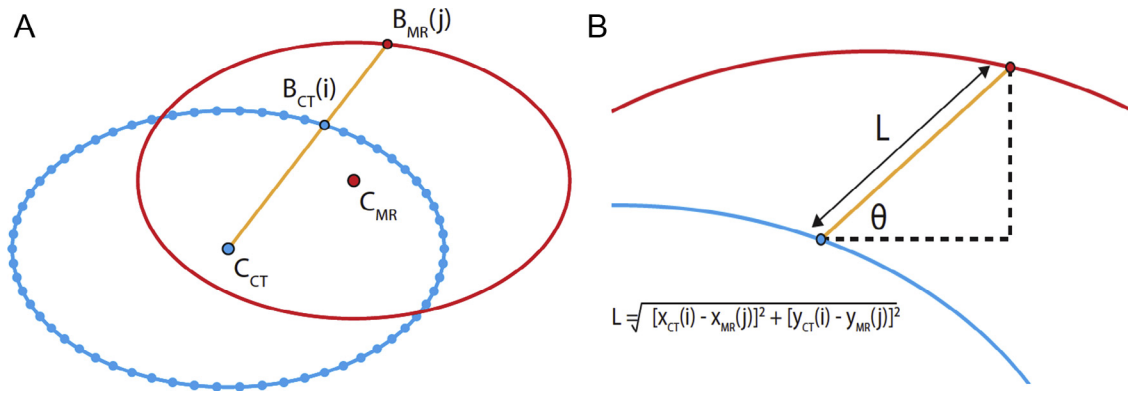

Figure 2 Margin quantification process. (a) For each magnetic resonance–based boundary point, $B_{MR}(j)$, outside of the computed tomography (CT)-based image mask, a segment is projected from the CT-based centroid, C_{CT}, through and beyond $B_{MR}(j)$. The intersection of the segment with the CT-based contour yielded point $B_{CT}(i)$. This process produces a segment, S_{ij}, defining a margin expansion in a particular direction. The length L_{ij} of S_{ij} can be determined from the component vectors $(S_{ij})_y$ and $(S_{ij})_x$. Likewise, the orientation θ can be determined from the inverse tangent of these component vectors: $\Theta = \arctan[(S_{ij})_y / (S_{ij})_x]$.

similar to the clinical anatomic landmarks of the thoracic inlet and inferior pulmonary vein. In this study, we further separated the esophageal segments into quadrants to provide a greater understanding of the potential for nonuniform esophageal margin expansion.

Segments were binned according to quadrant with $0° < \theta \leq 90°$, $90° < \theta \leq 180°$, $180° < \theta \leq 270°$, and $270° < \theta \leq 360°$, represented by the left anterior, right anterior, right posterior, and left posterior quadrants, respectively. A representative boundary measurement on an axial slice is shown in Figure 3.

Data were analyzed on both a pooled and individual patient basis. Population-based data are described by means among all measurements. For patient-specific data, we report the maximum measurement in each quadrant as the representative measure per quadrant per slice for the purposes of statistical analysis because we believe this measure to be the most important for inferring margins. Sample means were compared by analysis of variance. Statistical calculations were done in Microsoft Excel (Redmond, WA).

Results

Three on-treatment MRI scans for each of the 7 patients were evaluated. These images provided a total of 1629 axial slices for measurement, ultimately yielding 84,716 total measurements (differences in contour boundaries). A movie demonstrating the algorithm processing an entire volume is presented in the supplementary materials.

The mean esophageal measurements (with 95% confidence intervals) were 5.2 ± 0.03 mm, 4.0 ± 0.03 mm, and 3.7 ± 0.03 mm for the lower, middle, and upper esophagus,

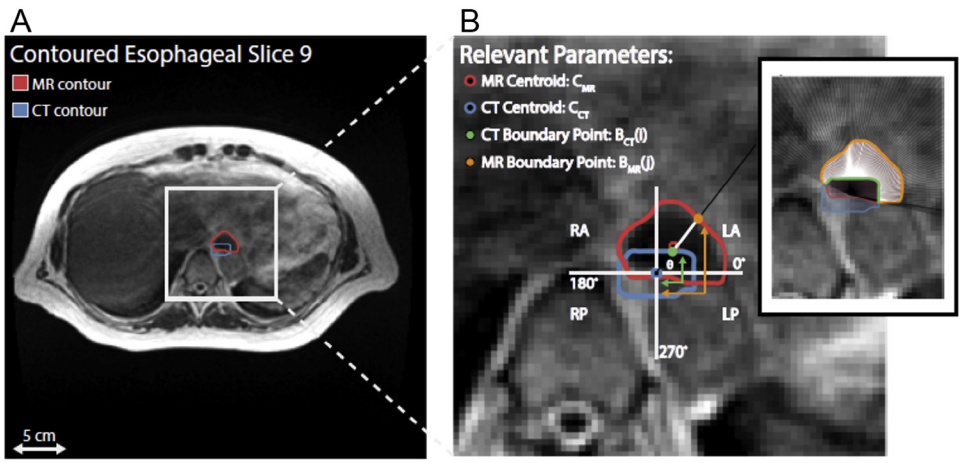

Figure 3 (a) An axial slice is depicted with computed tomography (CT)-based contour (blue) and magnetic resonance (MR)-based contour (red) overlaid. (b) Using the CT contour centroid (C_{CT}) as the origin, a line segment is projected through an MR boundary point (B_{MR}) and the intersection with the CT contour, B_{CT}, is found.

Table 2 Mean comparison of different esophageal segment measurements (in mm)

Statistic	Lower	Middle	Upper	Groups	*P*-value
Mean	5.2	4.0	3.7	Lower esophagus, upper esophagus	<.001
95th percentile	11.5	9.5	9.1	Middle esophagus, upper esophagus	<.001
SD	3.4	2.7	2.6	Lower esophagus, middle esophagus	<.001
#Obs	36363	25745	22607		
95%Cl	0.03	0.03	0.03		

#Obs, number of observations; CI, confidence interval; SD, standard deviation.
Upper, middle, and lower refer to the segments of the esophagus. The data are based on a composite of the 3 separate magnetic resonance image sets per patient for all 7 patients. In this analysis, the planning computed tomography image simulation scan is considered the ground truth. By an analysis of variance, there is a statistically significant difference in the magnitude of measurements between different esophageal-defined segments.

respectively. The lower esophagus exhibited the greatest magnitude of variation. However, there was a statistically significant difference in the means among all segments on analysis of variance. Table 2 summarizes these data.

In the lower esophageal segment, the mean measurements in the left anterior, left posterior, right anterior, and right posterior were 5.2 ± 0.07 mm, 6.0 ± 0.09 mm, 4.8 ± 0.08 mm, and 5.1 ± 0.08 mm, respectively. A complete summary of quadrants by segment measurements is shown in Table S3 of the supplementary materials.

Patient-specific esophageal variability

There was considerable interpatient variability with regard to esophageal motion. For patient-specific data, we report the maximum measurements per quadrant per esophageal segment. A full description of patient-specific data is given in Tables S4 and S5 of the supplementary materials.

In the lower esophageal segment, patients 1 and 4 exhibited the greatest motion in the left anterior quadrant (16.5 mm and 20.9 mm, respectively). Patients 4 and 6 exhibited the greatest motion in the right anterior quadrant (18.1 mm and 14.2 mm, respectively). Patients 7 and 3 exhibited the greatest motion in the right posterior quadrant (18.8 mm and 13.5 mm, respectively). Patients 7 and 3 exhibited the greatest motion in the left posterior quadrant (16.8 mm and 13.8 mm, respectively (measurements of 0 do not necessarily imply that boundaries superimpose but rather that the MR contour is completely contained within a CT contour for a specific quadrant). Figure 4 graphically represents the maximum margin for all fractions considered for each patient.

Discussion

In this small study, we have described a novel, computation-based method for assessing esophageal motion that can quickly identify the maximum change in contour boundary in any orientation in the axial plane, from which patient-specific treatment margins can readily be derived in an SBRT treatment plan.

Other prior methods to evaluate esophageal motion using digital calipers to measure anterior-posterior and medial-lateral motion on CT images are much more cumbersome and impractical to use during an adaptive treatment process. In a recent study of esophageal motion between the sternal notch to 2 cm cranial to the gastroesophageal junction using 4-dimensional CT, Dieleman et al. reported greater mobility in the distal esophagus compared with the proximal esophagus, with mediolateral margins of 9 mm and dorsoventral margins of 8 mm being sufficient to account for all such mobility at the distal esophagus for esophagus cancer treatment planning.[6]

Additional dosimetric studies have been reported. Cohen et al. assessed inter- and intrafractional esophageal motion by comparing simulation CT with CT-on-rails imaging before and after radiation therapy. Their data suggest that 95% of esophageal mobility would be accounted for with margin expansions of 12 mm leftward, 8 mm rightward, 10 mm posterior, and 9 mm anterior.[9] Palmer et al. studied the displacement of the esophagus secondary to the cardiac cycle from the carina to the caudal aspect of the heart. This study tracked the voxel-for-voxel trajectory of the esophagus and showed that displacement was patient specific with transverse displacements of up to 10 mm.

Similar to prior studies, we also report that the greatest magnitude of motion occurs in the lower esophagus, compared with the mid- and upper esophagus. The position of the esophagus is influenced by respiratory and cardiac motion as well as deglutination.[1] The motion of the diaphragm during the respiratory cycle likely cause flexure of the lower esophagus, which results in a greater degree of movement. On the basis of this small population data series, 95% of mobility in the lower esophagus would be accounted for through adoption of treatment margins of 10.1, 11.5, 8.5, and 9.8 mm in the left anterior, left posterior, right anterior, and right posterior quadrants, respectively. Importantly, our patient-specific measurements suggest that population-based margins may prove to be too restrictive for some patients and insufficient for others. Therefore, an individualized approach is required for adaptive SBRT treatments to reduce toxicity and improve tumor control.

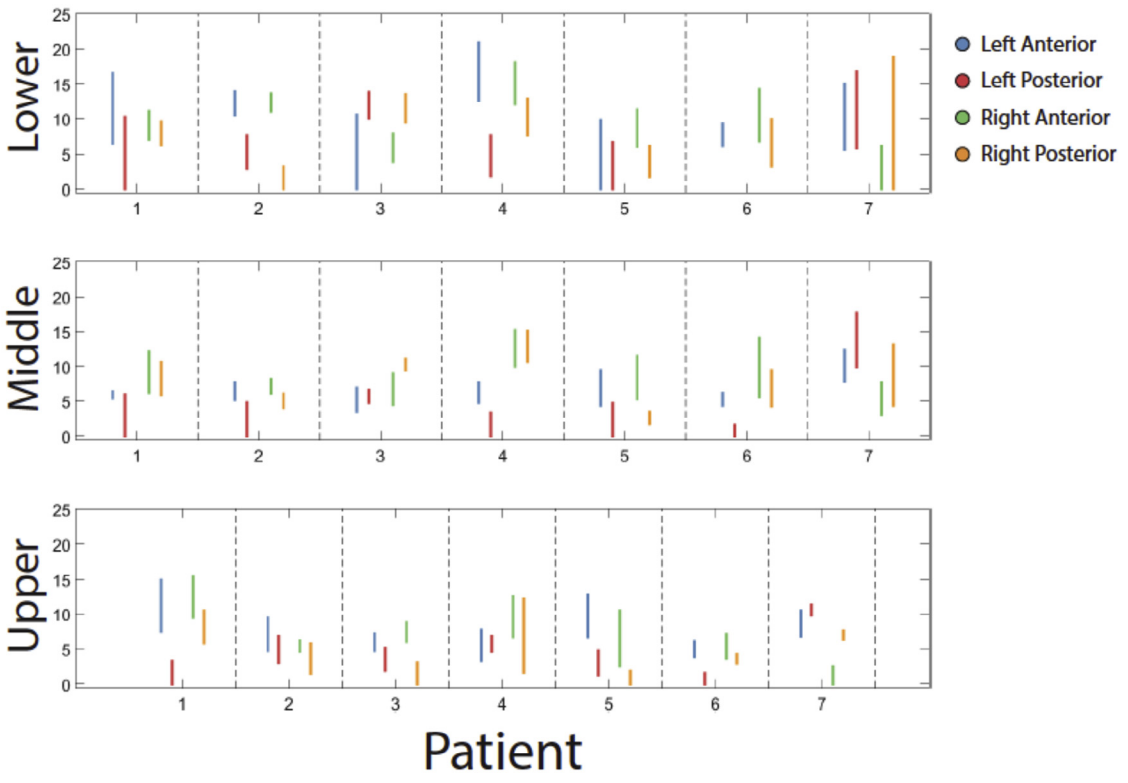

Figure 4 Bars denote the range of maximum measurements (in mm) for all fractions considered for each patient. Upper, middle, and lower refer to the segments of the esophagus. Note that each measurement has an uncertainty of approximately ±1.5 mm because the in-plane image resolution on the magnetic resonance data is 1.5×1.5 mm^2.

There are several limitations to this study, including the small number of cases and the inability to identify the specific phases of the respiratory cycle on the MRI scans because these were acquired during free breathing. Future studies using gated MRI scans to evaluate the relationships between esophagus position and specific phases of the respiratory cycle are being pursued. Additionally, methods to align the images have the potential to influence the measurements of esophageal motion. In previously published studies,[10,12] alignment using bony anatomy has been shown to be a consistent, reproducible, and clinically relevant means for assessing esophageal displacement across all fractions and in all patients. We used a reliable registration method to obtain figures-of-merit of esophageal motion to evaluate a novel MATLAB-based clinical tool.

Conclusions

The lower esophagus exhibits the greatest magnitude of mobility compared with the middle and upper segments. A novel computational-based approach enables personalized, nonuniform esophageal margins to be tailored to individual patients. With a trend toward increased use of large fraction, SBRT treatment planning combined with targeted therapies as well as greater emphasis on mitigating potential complications to normal tissues is required during the planning process. Future work will apply this method to 4-dimensional MRI data for a robust assessment of intrafractional esophageal motion and the dosimetric implications of this motion. We are in the process of evaluating this computational-based method of identifying nonuniform normal tissue margins in relation to other critical structures that are subject to movement, including the spinal cord.

Supplementary data

Supplementary material related to this article can be found at https://doi.org/10.1016/j.adro.2017.10.003.

References

1. Machtay M, Hsu C, Komaki R, et al. Effect of overall treatment time on outcomes after concurrent chemoradiation for locally advanced non–small-cell lung carcinoma: Analysis of the Radiation Therapy Oncology Group (RTOG) experience. *Int J Radiat Oncol Biol Phys*. 2005;63:667-671.

2. Ahn SJ, Kahn D, Zhou S, et al. Dosimetric and clinical predictors for radiation-induced esophageal injury. *Int J Radiat Oncol Biol Phys*. 2005;61:335-337.
3. Werner-Wasik M, Yorke E, Deasy J, Nam J, Marks LB. Radiation dose-volume effects in the esophagus. *Int J Radiat Oncol Biol Phys*. 2010;76:S86-S93.
4. Nuyttens JJ, Moiseenko V, McLaughlin M, Jain S, Herbert S, Grimm J. Esophageal dose tolerance in patients treated with stereotactic body radiation therapy. *Semin Radiat Oncol*. 2016;26:120-128.
5. Wu AJ, Williams E, Modh A, et al. Dosimetric predictors of esophageal toxicity after stereotactic body radiotherapy for central lung tumors. *Radiother Oncol*. 2014;112:267-271.
6. Cox BW, Jackson A, Hunt M, Bilsky M, Yamada Y. Esophageal toxicity from high-dose, single-fraction paraspinal stereotactic radiosurgery. *Int J Radiat Oncol Biol Phys*. 2012;83:e661-e667.
7. Stephans KL, Djemil T, Diaconu C, et al. Esophageal dose tolerance to hypofractionated stereotactic body radiation therapy: Risk factors for late toxicity. *Int J Radiat Oncol Biol Phys*. 2014;90:197-202.
8. Dieleman EM, Senan S, Vincent A, Lagerwaard FJ, Slotman BJ, van Sörnsen de Koste JR. Four-dimensional computed tomographic analysis of esophageal mobility during normal respiration. *Int J Radiat Oncol Biol Phys*. 2007;67:775-780.
9. Yamashita H, Haga A, Hayakawa Y, et al. Patient setup error and day-to-day esophageal motion error analyzed by cone-beam computed tomography in radiation therapy. *Acta Oncol*. 2010;49:485-490.
10. Good E, Oral H, Lemola K, et al. Movement of the esophagus during left atrial catheter ablation for atrial fibrillation. *J Am Coll Cardiol*. 2005;46:2107-2110.
11. Cohen RJ, Paskalev K, Litwin S, Price R, Feigenberg SJ, Konski A. Esophageal motion during radiotherapy: Quantification and margin implications. *Dis Esophagus*. 2010;23:473-479.
12. Palmer J, Yang J, Pan T, Court LE. Motion of the esophagus due to cardiac motion. *PLoS ONE*. 2014;9:e89126.
13. Noel CE, Parikh PJ, Spencer CR, et al. Comparison of onboard low-field magnetic resonance imaging versus onboard computed tomography for anatomy visualization in radiotherapy. *Acta Oncol*. 2015;54:1474-1482.
14. Mutic S, Dempsey JF. The ViewRay system: Magnetic resonance-guided and controlled radiotherapy. *Semin Radiat Oncol*. 2014;24:196-199.